Numerical prediction of aerodynamic loads acting on a blade section-model oscillating in stall

Nicolas Cortes, Xavier Amandolese, Jean Lou Pfister, Frédéric Blondel, Ronan Boisard, Jean-Sébastien Schotté, Y. Mauffrey

Numerical prediction of aerodynamic loads acting on a blade section-model oscillating in stall

Journal of Physics: Conference Series **2767** (2024) 022014 doi:10.1088/1742-6596/2767/2/022014

Numerical prediction of aerodynamic loads acting on a blade section-model oscillating in stall

N Cortes[1,2,3], X Amandolese[3], JL Pfister[2], F Blondel[2], R Boisard[1], JS Schotté[1], Y Mauffrey[1]

[1] DAAA, ONERA, Université Paris-Saclay, France
[2] IFP Energies nouvelles, 1 et 4 Avenue de Bois-Préau, 92852 Rueil-Malmaison, France
[3] LMSSC, Conservatoire National des Arts et Métiers, Paris, France

E-mail: cortes.nicolas@onera.fr, xavier.amandolese@lecnam.net, jean-lou.pfister@ifpen.fr, ronan.boisard@onera.fr

Abstract. For blades operating close to stall angle of attack, one of the potential instabilities is known as stall flutter. It is a dynamic instability in torsion for which the mechanism of energy transfer relies on a dynamic stall process where the flow separates partially or completely during each cycle of oscillation. It leads to dynamic loops in lift, drag and moment that affect the aerodynamic performance of the blade, create unsteady stresses in the blades and can lead to fatigue damage. In the present study, dynamic loops of a NACA 63_4421 airfoil in forced pitch oscillations have been simulated with the FastS CFD solver based on a URANS modelling approach and compared to benchmark experiments as well as results obtained with the ONERA semi-empirical dynamic stall model using a unique set of dynamic parameters that best fit the experimental dynamic loops. The dynamic tests have been conducted for a mean angle of attack of 13.5°, an amplitude of oscillation of 8° and three reduced frequencies $k_1 = 0.0183$, $k_2 = 0.0785$ and $k_3 = 0.183$. This study has shown that the CFD FastS solver can satisfactorily reproduce the unsteady lift and moment coefficients experienced by a section model oscillating in stall.

1. Introduction

Wind turbines are becoming increasingly larger, as a way to improve the cost effectiveness of wind energy. This new generation of wind turbines leads the designer to develop slender blades for which unsteady aerodynamic loading and aeroelastic instabilities are a matter of great concern. For blades operating close to stall angle of attack, a potential instability known as *stall flutter* may develop. It is a dynamic instability in torsion for which the mechanism of energy transfer relies on a dynamic stall process where the flow separates and reattaches partially or completely during each cycle of oscillation [1]. It leads to dynamic loops in lift, drag and moment that affect the aerodynamic performance of the rotor, create unsteady stresses in the blades and can lead to fatigue damage on the turbine. Many studies have been realised in the past on stall-induced vibrations experienced by stall-regulated wind turbines in normal condition [2, 3, 4]. But recently, stall-induced vibrations occurring on parked positions are under focus [5, 6, 7].

Dynamic stall has first been observed on wings and helicopter blades. Early experimental investigations have been conducted to draw a first description of the phenomenon for thin airfoils [8, 9]. Thicker airfoils representative of wind turbine airfoils have also been experimentally studied (see for example Ramsay et al. [10], Amandolese and Szechenyi [11])

As CFD approaches can provide detailed spatial and temporal information, it is a promising way to investigate dynamic stall. Several numerical studies have been conducted in which the blade motion is imposed. Good agreement between numerical and experimental data has been obtained for the dynamic loops of the S809 airfoil in [12]. Bangga et al. [13] have simulated other loops of the same airfoil and obtained similar results. They however pointed out the importance of the turbulence model as it has impact on the flow structures. The Spalart-Allmaras model seems to show better prediction than the SST model. The effect of the turbulence intensity on dynamic stall of the NACA 0012 airfoil has been studied by Kim et al. [14]: by using LES they found that the minimum moment decreases with the increase of freestream turbulence.

With the increase of numerical capacities, it is possible to simulate dynamic stall with higher fidelity. Visbal et al. [15] and Benton et al. [16] performed LES simulation of a NACA 0012 airfoil. They depicted the complex interaction between the turbulent-separation vortex (TSV) and the leading edge vortex (LEV) that produces the dynamic stall vortex (DSV). Huang at al. [17] have used high fidelity LES to investigate the impact of freestream turbulence on dynamic stall of the ClarkY airfoil. They found that the turbulence increases the lift coefficient during the downstroke because of an accelerated flow attachment during the downstroke. Damiola et al. [18] have experimentally investigated the influence of turbulence intensity on the dynamic stall of a NACA 0018 airfoil. They observed the enhanced flow reattachment during downstroke and a delayed flow separation during upstroke.

To compute dynamic stall induced loads with lower cost, semi-empirical dynamic stall models have also been developed [19, 20]. Useful in pre-design process, these models however need to be calibrated over dedicated section model tests.

In that context, the objective of this paper is to validate the capability of the CFD solver FastS to capture the dynamic stall process of a thick section model blade, representative of wind turbine airfoils, forced to oscillate in pitch. FastS results will be compared to experiments performed on a NACA 63_4421 airfoil and with the results obtained with the ONERA semi-empirical dynamic stall model. This validation is a first step before studying more complex cases of stall induced vibrations over a wind turbine blade.

2. Methodology

2.1. Benchmark experiments

The experimental reference data previously published in [11] were obtained from static and dynamic section model tests performed on a NACA 63_4421 section model in a $5m \times 3m$ wind tunnel, for Reynolds numbers, $Re = \frac{Uc}{\nu} = 10^6$, using an experimental rig which forces the section model to oscillate in pitch, around its fore quarter-chord axis, at different values of mean angle of attack $\bar{\alpha}$, reduced frequency $k = \frac{\pi f c}{U}$ and amplitude of motion $\tilde{\alpha}$. The aerodynamic lift, drag and pitching moment about the quarter chord were obtained through unsteady surface pressure measurements (see [11] for further information on the experimental process and results).

As the FastS CFD solver assumes a fully turbulent boundary layer over the blade section, numerical predictions will be compared with the experimental results obtained for a grid turbulence intensity $Tu = 4\%$. As shown in figure 3.1, the FastS steady results in lift perfectly match the experiments for $Tu = 4\%$.

2.2. CFD solver : FastS

Fluid dynamic simulations have been done with the solver FastS developed at ONERA [21]. It is a research solver optimised for structured meshes that can perform URANS, LES and URANS/LES simulations. For the present study only 2D URANS simulations were conducted. The compressible Navier–Stokes equations are solved using a finite volume AUSM+(P) spatial discretization scheme of the fluxes [22] that overcomes the numerical stiffness of the compressible Navier–Stokes equations at low Mach number. The temporal scheme used in FastS is the

Gear scheme which is an implicit predictor-corrector method solved with dual time stepping (DTS) approach. The turbulence is modeled with the Spalart-Allmaras model [23] which seems adequate for dynamic stall according to [13]. To account for the pitching motion of the airfoil, the mesh is rotated around the quarter chord in a rigid fashion.

The simulated case consists of a NACA 63_4421 airfoil with a 0.5m chord immersed in a reference flow of 30m/s. It corresponds to a Reynolds number $Re = 10^6$ and Mach $M = 0.05$.

2.3. Numerical discretisation

A CFD mesh of the NACA 63_4421 was generated with Construct2D. A O-grid type mesh is used. A convergence study on both the domain size and the number of points has been realised, leading us to generate a mesh with a diameter of 1000 chords composed of 10^5 points. To describe the boundary layer, the first cell height is small enough to satisfy an y^+ value lower than one. The outer limit of the CFD domain has been defined as a farfield boundary condition.

A total of 50 000 time-steps per period of oscillation were required to achieve the convergence of the dynamic stall loops for $k_2 = 0.0785$ and $k_3 = 0.183$ whereas 100 000 time-steps by period has been necessary for $k_1 = 0.0183$ (It corresponds to a flow displacement of 0.002 chord by time-steps).

2.4. ONERA dynamic stall model

The ONERA dynamic stall model is a semi-empirical set of differential equations developed by Tran and Petot [19] and improved by Petot [24]. It is based on the airfoil steady characteristics (steady lift, drag and moment coefficient evolution with the angle of attack) and a set of parameters that need to be identified using dynamic tests. The parameters have been set manually to fit the experimental results as much as possible. In the present study the lift, drag and moment formulations proposed in [25] have been used with the coefficients given in Table 1.

Table 1. Coefficients used in the ONERA model

Coefficient	Value	Coefficient	Value	Coefficient	Value	Coefficient	Value
σ_{1_l}	-0.1	σ_{1_m}	-0.1	r_{0_l}	0.175	r_{0_m}	0.1
a_{0_l}	0.25	a_{0_m}	0.1	r_{2_l}	0.04	r_{2_m}	0.1
a_{2_l}	0.15	a_{2_m}	0.1	E_{2_l}	-0.1	E_{2_m}	60
$\Delta\tau_{d_l}$	4	$\Delta\tau_{d_m}$	0				
β	$\sqrt{1-M^2}$	α_l	$0.6 + 0.25(\beta - 1)$	σ_l	$3\pi/\beta$	d_l	$0.6\sigma_{1_l}\lvert\Delta c_l\rvert$

3. Results and discussion for fixed-wing cases

3.1. Static polars

In this section, 2D unsteady RANS simulations were conducted so as to calculate the aerodynamic lift and moment time-averaged polar curve. The data points have been gathered by successive steps of angle of attack. For each angle of attack, the transient regime induced by increasing the step angle of attack has been ignored and the mean aerodynamic coefficients have been computed over $25\frac{c}{U} = 0.4167$ seconds. Results are reported in figure 3.1.

The experimental results from [11] are reported with blue plain circle. Plain circle in black are used for the FastS-full results for which coefficients were calculated with a full integration of the stress over the airfoil using all the surface mesh point. FastS-exp results, reported with orange plain square, are computed using the same integration method as the experiment. Regarding the lift coefficient, FastS-full and FastS-exp results are very close and well reproduce the lift

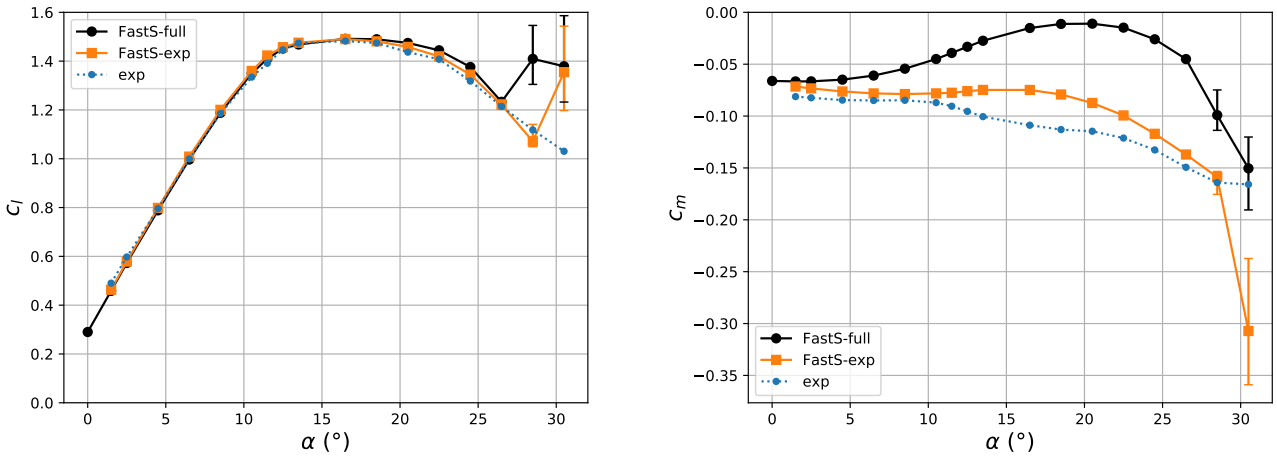

Figure 1. Steady lift coefficient (left) and moment coefficient about the quarter chord (right) results. FastS-full is obtained with a full integration of the stress over the airfoil while FastS-exp is calculated using the same integration method as the experiment [11].

coefficient evolution for angles of attack up to 26°. For higher angles of attack, the mean lift coefficient is overestimated and unsteady behavior is observed. In this region, the flow is fully detached and CFD exhibits vortices that are alternatively emitted from the leading and trailing edge into the wake, leading to a strong unsteady aerodynamic load and an increase of the mean value of the lift coefficient. Note that the frequency of the vortex emission observed here is coherent with the one expected for the Von Kármán vortex street downstream a planar plate in incidence [26]. No mention of this unsteady behavior and its impact on the steady results has however been reported in [11].

Regarding the moment coefficient about the quarter chord, significant discrepancies can be observed between the experiments and FastS-full results (full integral of stress over the airfoil). While experimental results show a gradual decrease of the moment coefficient beyond 10°, FastS-full results show an increase up to 20°, with an inflexion point close to 7°, followed by a fall down of the moment coefficient that is abrupt for angle of attack beyond 26° where a strong unsteady vortex wake signature was observed. Using the same integration method as the experiment, i.e. using the pressure at the same positions as the pressure taps of the experiment, numerical predictions are closer to the experiment. This seems to show that the experiment was lacking of taps to correctly capture the impact of the dynamic stall fluid mechanism on the moment coefficient.

3.2. C_p curves

The remaining difference between experiments and FastS-exp results can be understood by looking at the pressure coefficient curves. In figure 2, the pressure data from the CFD (FastS-exp) are compared to the experimental pressure data for three angles of attack: 1.5°, 11.5° and 24.5°.

At 1.5° of angle of attack, the simulation underestimates depression in both the upper and lower surfaces of the airfoil. It does not affect the lift coefficient and slightly underestimates the negative moment coefficient about the quarter chord. At 11.5°, the pressure coefficient is well predicted. However, a deviation appears at the upper surface near the trailing edge. The lift is balanced by a disagreement around the quarter chord of the lower surface. However, it causes the moment to diverge even more from the experimental data. At 24.5°, a large part of

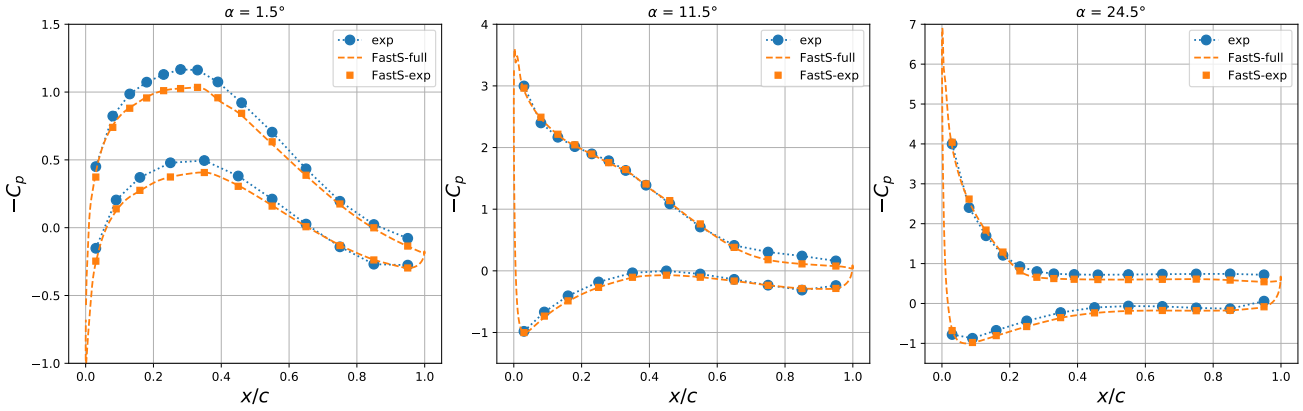

Figure 2. Mean pressure coefficient comparison between simulation (FastS-exp, FastS-full) and experiment (exp) for three angles of attack.

the upper surface is stalled – corresponding to the constant C_p area. In this region, the CFD code predicts slightly lower values of $-C_p$ than the experiment. It appears to be the reason of the major misalignment in the curve of moment coefficient.

By looking at the leading and trailing, it can be notice that important values of C_p in FastS-full are not measured by the experiment. The large value of C_p at the leading edge for $\alpha = 24.5°$ causes an increase of the moment. Therefore, greater number of taps in the leading and trailing edge should improve the measure of the moment.

4. Results and discussion for oscillating-wing cases

Tests with an oscillating wing have been simulated using the CFD FastS solver for $\bar{\alpha} = 13.5°$, $\tilde{\alpha} = 8°$ and three different reduced frequencies $k_1 = 0.0183$ (slow oscillation), $k_2 = 0.0785$ and $k_3 = 0.183$ (fast oscillation). The airfoil is forced to oscillate in pitch around its quarter chord following the expression :

$$\alpha = \bar{\alpha} + \tilde{\alpha} \sin(2\pi f t) \tag{1}$$

where the frequency f is chosen so as to match the prescribed reduced frequency.

In this section experiments with be compared with the results obtained using the ONERA dynamic stall model and FastS-exp results for which the lift an moment coefficients are computed using the same integration method as the experiment.

4.1. Dynamic loops

Unsteady lift coefficient results are compared with experiments in the top of figure **??** along with the results obtained with the ONERA dynamic stall model using a unique set of dynamic parameters that best fit the experimental dynamic loops. For $k_1 = 0.0183$ and $k_2 = 0.0785$, both the FastS solver and the dynamic stall model correctly reproduce the experimental loops. For the highest reduced frequency ($k_3 = 0.183$), the loop obtained with the CFD solver is still very close to the experimental one while the ONERA dynamic stall model produces a loop for which the lift coefficient is significantly reduced in the end of the stalled regime.

Unsteady moment coefficient results are compared with experiments in the bottom of figure 3. As the experimental static curves was used to compute the ONERA dynamic stall model, the loops obtained with this model are closer to the experiment. For $k_1 = 0.0183$ and $k_1 = 0.0785$, the loops are in good agreement with the experiment. However, for $k_3 = 0.183$, the ONERA

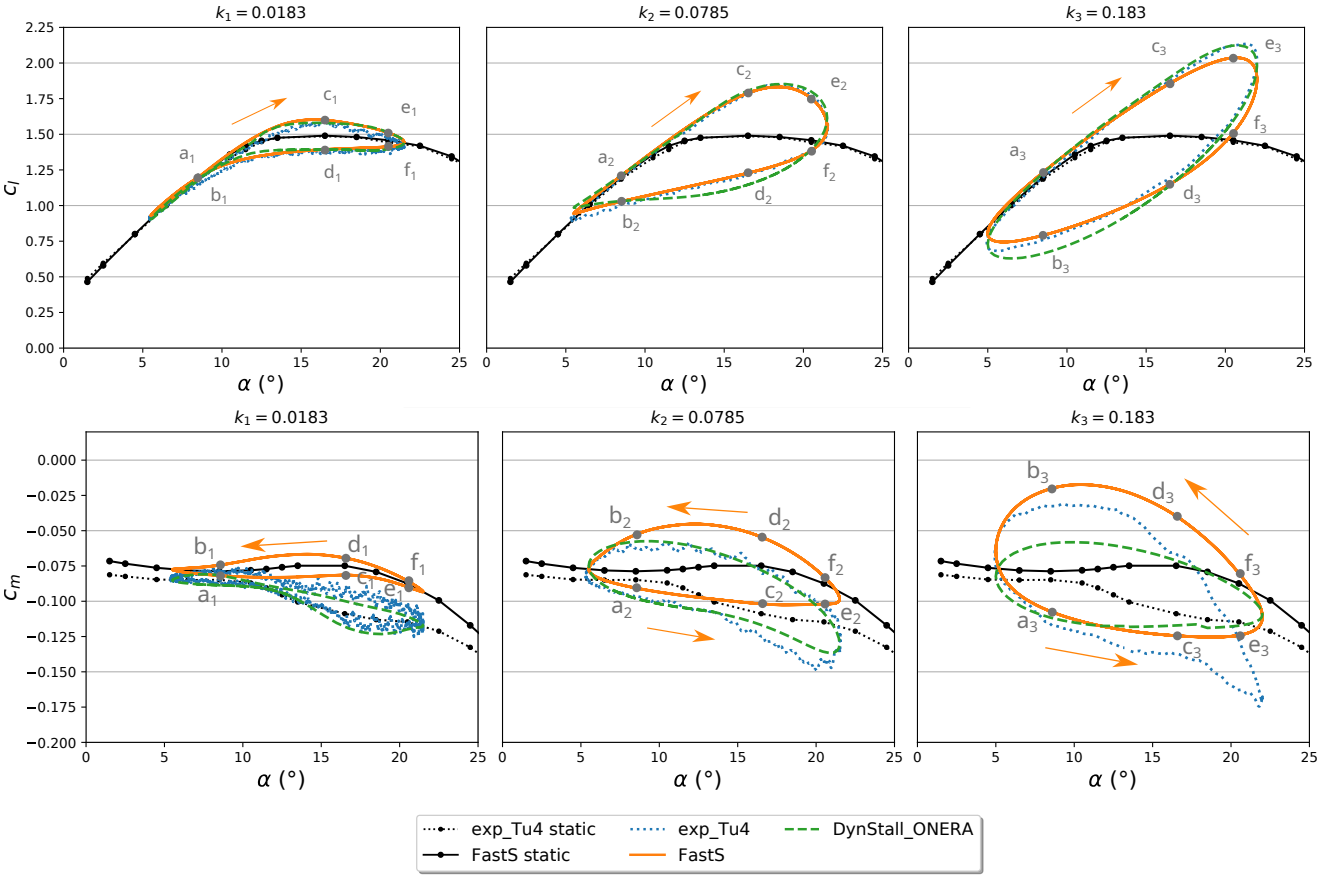

Figure 3. Static and dynamic lift coefficients (top) and moment coefficients (bottom) for three reduced frequencies; comparison of numerical predictions (FastS-exp and Onera dynamic stall model) with experiments reported in [11]. The lift loops turn clockwise while the moment loops turn counter-clockwise. The letters indicate specific states used in the following figures.

dynamic stall model underestimates the size and area of the loop and fails to capture the minimum of the moment coefficient occurring at the maximum angle of attack. Because of the discrepancies between the static curves of FastS and the experiments, the dynamic loops obtained with FastS significantly departs from the experiments. However their dynamic behaviours in regards to the associated steady curve are coherent.

4.2. Pressure coefficient

Numerical predictions of the pressure coefficients C_p associated to the dynamic loops for $k_1 = 0.0183$, $k_2 = 0.0785$ and $k_3 = 0.183$ are reported in figure 4 for three different angles of attack.

At $\alpha = 8.5°$, for $k = 0.0183$ the C_p curve in downstroke coincides with the static curve, meaning that the dynamics are sufficiently slow for the flow to have time to reattach. But for higher reduced frequency, the flow is still partly stalled. For all the reduced frequency studied, the C_p curves in upstroke are, in the major part, overlapping the static curve. There is a little difference in the upper surface, i.e. the suction surface, near the leading edge, where the depression is slightly reduced increasing the reduced frequency.

At $\alpha = 16.5°$, the flow is partialy stalled for all the reduced frequencies but the position of the stall point depends on the reduced frequency. During the upstroke, the position of the stall point

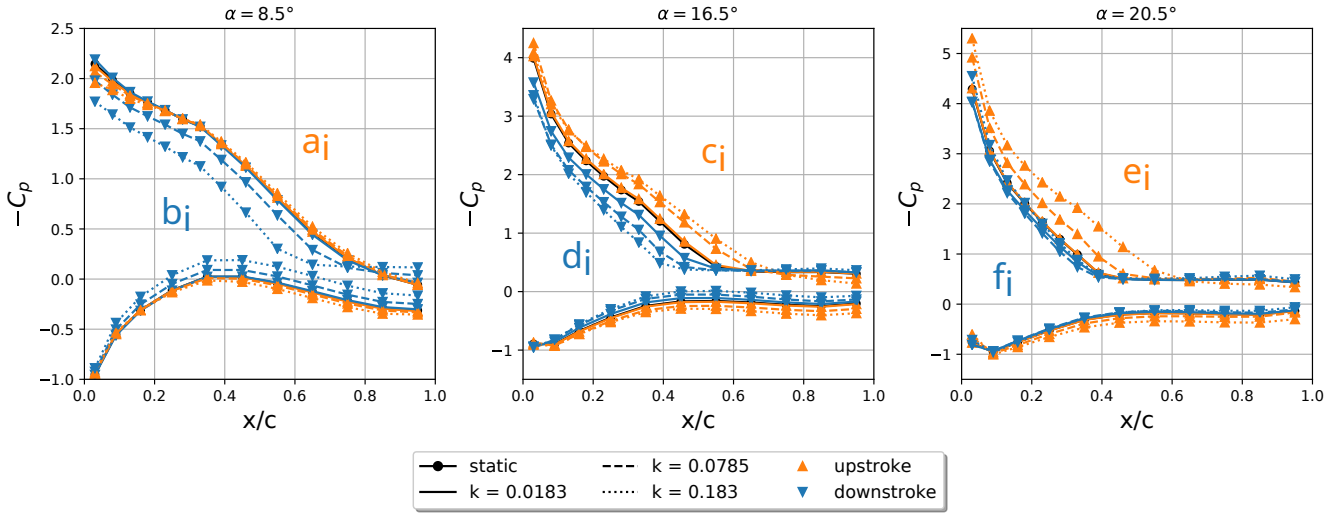

Figure 4. Pressure coefficient (FastS-exp results) associated to the dynamic for the three reduced frequency at three angles of attack. The pressure coefficients are represented during the upstroke and the downstroke.

is closer to the trailing edge compared to the static situation whereas during the downstroke, it is closer to the leading edge. This indicates that the stall phenomenon experiences delays during the loop. Moreover, this delay is increasing with the reduced frequency. For the lower surface, i.e. the pressure surface, the pressure is higher compared to the static during the upstroke whereas the pressure is lower during the downstroke. This effect is increased by the rise of the reduced frequency.

At $\alpha = 20.5°$, the C_p curves are close to the static one during the downstroke. It means that the dynamic effect in this part of the loops is limited. During the upstroke, the stall delay is still visible.

4.3. Fully resolved flow field

The dynamic flow field is discussed in this section. Vorticity field is displayed for the reduced frequency $k_3 = 0.183$ in figure 5. As it has been identified with the C_p-curves, the snapshots show the delay for the flow to reattach. Clear differences in the vorticity field can be observed between the upstroke and the downstroke for a same angle of attack. The pressure gradient helps the flow to stay longer attached during the upstroke while it encourages stall during the downstroke. However, for the range of angles of attack under study, the stall point has never reached the leading edge and no shedding of leading edge dynamic stall vortex has been observed.

4.4. Damping

The snapshots emphasize a dissymmetry of the flow field between the upstroke and the downstroke leading to aerodynamic loops in both lift and moment coefficients. This behaviour generates exchanges of energy between the flow and the structure. For aeroelastic considerations, it is important to know if the dynamic stall has a stabilising or destabilising effect on the oscillations. As the airfoil is forced to oscillate in pitch, the aerodynamic work is proportional to the area covered by the loop of the moment coefficient. Moreover, the loops are counter-clockwise for all the reduced frequency under study. It means that the flow is extracting energy from the structure, adding a positive damping to it.

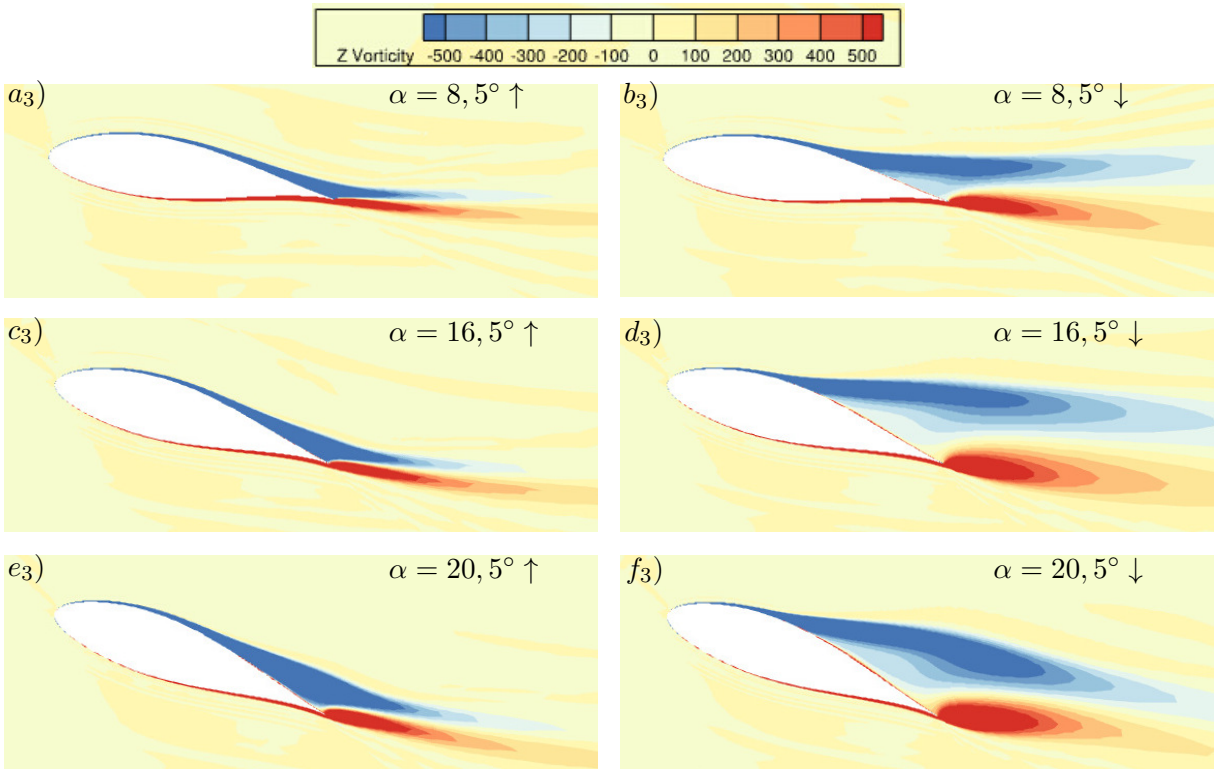

Figure 5. Snapshots of the vorticity field for the reduced frequency $k_3 = 0.183$ at three angles of attack during the upstroke (a_3, c_3, e_3) and the downstroke (b_3, d_3, f_3)

To quantify this damping, Carta and Niebanck [27] defined the dimensionless cycle aerodynamic damping as:

$$\Xi_{cycle} = -\frac{1}{\pi\tilde{\alpha}^2}\oint c_m d\alpha. \tag{2}$$

This dimensionless aerodynamic damping has been calculated for the experiments and simulations. The results are reported in figure 6 along with the dimensionless aerodynamic damping computed from Theodorsen's linear formulation of the motion induced moment coefficient about the quarter-chord [28]. Theodorsen's theory predicts a positive dimensionless damping proportional to the reduced frequency. Although, neither the airfoil nor the movement fulfill the assumptions of Theodorsen linear theory (thin airfoil, small amplitude, potential flow), both the experimental and numerical results are consistent with it.

Using the same integration method as the experiment FastS-exp aerodynamic damping ratios are in the vicinity of the experimental damping for $k_1 = 0.0183$ and $k_2 = 0.0785$. However, for $k_3 = 0.183$, the dimensionless aerodynamic damping is approximately 45 % higher than the experimental one. Using a full integration of the stress over the airfoil FastS-exp, dimensionless aerodynamic damping are significantly lower than the experimental one for $k_1 = 0.0183$ ($\approx$ 50 % lower) and $k_2 = 0.0785$ ($\approx$ 30 % lower). However, for $k_3 = 0.183$ both the FastS-full and experiment dimensionless aerodynamic damping are very close.

5. Conclusion

This work focused on the dynamic stall behaviour of a thick airfoil used in wind turbines and represents an important first step toward the validation of a 3D aeroelastic code for

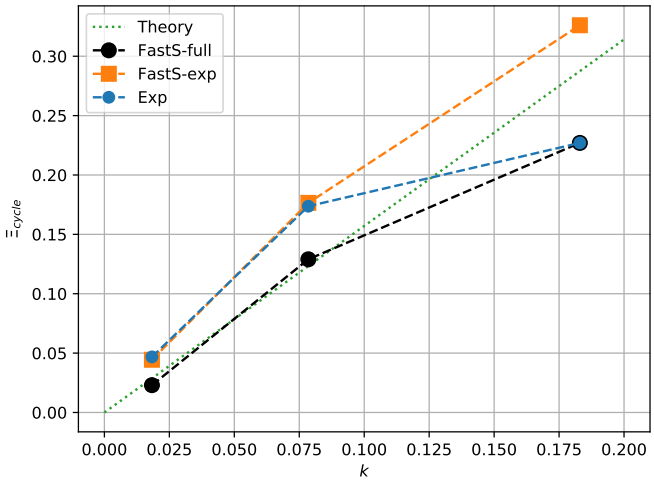

Figure 6. Dimensionless aerodynamic damping as a function of the reduced frequency.

wind turbines. To this end, the dynamic stall behaviour of a NACA 63_4421 airfoil has been investigated under pitching oscillations of mean angle of attack $\bar{\alpha} = 13.5°$ and amplitude $\tilde{\alpha} = 8°$ for three different reduced frequencies $k_1 = 0.0183$, $k_2 = 0.0785$ and $k_3 = 0.183$. The dynamic stall was simulated using a URANS solver with the Spalart-Allmaras turbulence model. The simulation results were confronted against experiment and the semi-empirical ONERA dynamic stall model. The lift coefficient loops were satisfactorily reproduced. Regarding the moment coefficient, discrepancies observed on the static and dynamic results were partially overcome using the same integration method as the experiment, i.e. using the pressure at the same positions as the pressure taps of the experiment. Using the FastS simulation, the dynamic behaviour of the flow has also been inspected. The delayed behaviour of the dynamic stall was highlighted by looking at pressure coefficients and vorticity field.

Finally, the dimensionless aerodynamic damping was calculated for the simulation and the experiment. A positive dimensionless aerodynamic damping almost proportional to the reduced frequency was observed. Results also showed that numerical simulations could help to better capture the moment coefficient loops and associated aerodynamic damping as a full integration of the stress over the airfoil can be computed.

References

[1] E. Dowell, R. Clark, D. Cox, H. Curtiss, J. Edwards, D. Peters, R. Scanlan, E. Simiu, F. Sisto, K. Hall, *et al.*, "A modern course in aeroelasticity," *A Modern Course in Aeroelasticity*, 2004.

[2] P. Lundsager, H. Petersen, and S. Frandsen, *The Dynamic Behaviour of the Stall-regulated Nibe a Wind Turbine: Measurements and a Model for Stall-induced Vibrations*. Risø National Laboratory, 1981.

[3] V. Riziotis, S. Voutsinas, E. Politis, and P. Chaviaropoulos, "Aeroelastic stability of wind turbines: the problem, the methods and the issues," *Wind Energy: An International Journal for Progress and Applications in Wind Power Conversion Technology*, vol. 7, no. 4, pp. 373–392, 2004.

[4] P. Chaviaropoulos, N. Soerensen, M. O. L. Hansen, I. Nikolaou, K. Aggelis, J. Johansen, M. Gaunaa, T. Hambraus, H. F. von Geyr, C. Hirsch, *et al.*, "Viscous and aeroelastic effects on wind turbine blades. the viscel project. part ii: Aeroelastic stability investigations," *Wind Energy: An International Journal for Progress and Applications in Wind Power Conversion Technology*, vol. 6, no. 4, pp. 387–403, 2003.

[5] D. C. Bak, "Research in aeroelasticity efp-2006," 2007.

[6] N. N. Sørensen and S. Schreck, "Computation of the national renewable energy laboratory phase-vi rotor in pitch motion during standstill," *Wind Energy*, vol. 15, no. 3, pp. 425–442, 2012.

[7] W. R. Skrzypiński, M. Gaunaa, N. Sørensen, F. Zahle, and J. Heinz, "Self-induced vibrations of a du96-w-180 airfoil in stall," *Wind Energy*, vol. 17, no. 4, pp. 641–655, 2014.
[8] L. W. Carr, K. W. McAlister, and W. J. McCroskey, "Analysis of the development of dynamic stall based on oscillating airfoil experiments," tech. rep., National Aeronautics and Space Administration, 1977.
[9] W. J. McCroskey, K. W. McAlister, L. W. Carr, and S. Pucci, "An experimental study of dynamic stall on advanced airfoil sections. volume 1: Summary of the experiment," tech. rep., National Aeronautics and Space Administration, 1982.
[10] R. Ramsay, M. Hoffman, and G. Gregorek, "Effects of grit roughness and pitch oscillations on the s809 airfoil," tech. rep., National Renewable Energy Lab.(NREL), Golden, CO (United States), 1995.
[11] X. Amandolese and E. Széchényi, "Experimental study of the effect of turbulence on a section model blade oscillating in stall," *Wind Energy: An International Journal for Progress and Applications in Wind Power Conversion Technology*, vol. 7, no. 4, pp. 267–282, 2004.
[12] G. Yu, X. Zhu, and Z. Du, "Numerical simulation of a wind turbine airfoil: dynamic stall and comparison with experiments," *Proceedings of the Institution of Mechanical Engineers, Part A: Journal of Power and Energy*, vol. 224, no. 5, pp. 657–677, 2010.
[13] G. Bangga, "Numerical studies on dynamic stall characteristics of a wind turbine airfoil," *Journal of Mechanical Science and Technology*, vol. 33, pp. 1257–1262, 2019.
[14] Y. Kim and Z.-T. Xie, "Modelling the effect of freestream turbulence on dynamic stall of wind turbine blades," *Computers & Fluids*, vol. 129, pp. 53–66, 2016.
[15] M. R. Visbal and D. J. Garmann, "Analysis of dynamic stall on a pitching airfoil using high-fidelity large-eddy simulations," *AIAA Journal*, vol. 56, no. 1, pp. 46–63, 2018.
[16] S. Benton and M. Visbal, "The onset of dynamic stall at a high, transitional reynolds number," *Journal of Fluid Mechanics*, vol. 861, pp. 860–885, 2019.
[17] X. Huang, M. Albers, P. Meysonnat, M. Meinke, and W. Schröder, "Analysis of the effect of freestream turbulence on dynamic stall of wind turbine blades," *International Journal of Heat and Fluid Flow*, vol. 85, p. 108668, 2020.
[18] L. Damiola, M. F. Siddiqui, M. C. Runacres, and T. De Troyer, "Influence of free-stream turbulence intensity on static and dynamic stall of a naca 0018 aerofoil," *Journal of Wind Engineering and Industrial Aerodynamics*, vol. 232, p. 105270, 2023.
[19] C. Tran and D. Petot, "Semi-empirical model for the dynamic stall of airfoils in view of the application to the calculation of responses of a helicopter blade in forward flight," 1980.
[20] J. Leishman and T. Beddoes, "A semi-empirical model for dynamic stall," *Journal of the American Helicopter Society*, vol. 34, no. 3, pp. 3–17, 1989.
[21] C. Laurent, *Étude d'écoulements transitionnels et hors équilibre par des approches DNS et RANS.* PhD thesis, Ecole nationale supérieure d'arts et métiers-ENSAM, 2012.
[22] I. Mary, P. Sagaut, and M. Deville, "An algorithm for unsteady viscous flows at all speeds," *International journal for numerical methods in fluids*, vol. 34, no. 5, pp. 371–401, 2000.
[23] P. Spalart and S. Allmaras, "A one-equation turbulence model for aerodynamic flows," in *30th aerospace sciences meeting and exhibit*, p. 439, 1992.
[24] D. Petot, "Differential equation modeling of dynamic stall," *La Recherche Aerospatiale(English Edition)*, no. 5, pp. 59–72, 1989.
[25] G. Dimitriadis, *Introduction to nonlinear aeroelasticity.* John Wiley & Sons, 2017.
[26] R. D. Blevins, *Flow-induced vibration.* 1977.
[27] F. O. Carta, C. F. Niebanck, and U. T. C. S. C. S. A. DIV, "Prediction of rotor instability at high forward speeds. volume 3. stall flutter," *US Army Aviation Mater. Lab.: Fort Eustis, VA, USA*, 1969.
[28] T. Theodorsen, "General theory of aerodynamic instability and the mechanism of flutter," tech. rep., National Advisory Committee for Aeronautics. Langley Aeronautical Lab., 1949.